

Nitrogen-Doped Graphene and Its Iron-Based Composite as Efficient Electrocatalysts for Oxygen Reduction Reaction

Journal:	<i>ACS Nano</i>
Manuscript ID:	nn-2012-02674k.R3
Manuscript Type:	Article
Date Submitted by the Author:	08-Oct-2012
Complete List of Authors:	Parvez, Khaled; Max Planck Institute for Polymer Research, Yang, Shubin; Max Planck Institute for Polymer Research, Hernandez, Yenny; Max Planck Institute for Polymer Research, Winter, Andreas; University of Bielefeld, Turchanin, Andrey; Universität Bielefeld, Physics of Supramolecular Systems Feng, Xinliang; Max-Planck Institute for Polymer Research, Synthetic Chemistry Mullen, Klaus; Max-Planck-Institute for Polymer Research,

SCHOLARONE™
Manuscripts

Nitrogen-Doped Graphene and Its Iron-Based Composite as Efficient Electrocatalysts for Oxygen Reduction Reaction

*Khaled Parvez^a, Shubin Yang^a, Yenny Hernandez^a, Andreas Winter^b, Andrey Turchanin^b,
Xinliang Feng^{*a}, Klaus Müllen^{*a}*

^aMax Planck Institute for Polymer Research, Ackermannweg 10, D-55128 Mainz, Germany

^bFaculty of Physics, University of Bielefeld, Universitätsstr. 25, D-33615 Bielefeld, Germany.

*Address correspondence to muellen@mpip-mainz.mpg.de; feng@mpip-mainz.mpg.de

ABSTRACT

The high cost of platinum based electrocatalysts for the oxygen reduction reaction (ORR) has hindered the practical application of fuel cells. Thanks to its unique chemical and structural properties, nitrogen doped graphene (NG) is among the most promising metal-free catalysts for replacing platinum. In this work, we have developed a cost effective synthesis of NG by using cyanamide as a nitrogen source and graphene oxide as a precursor, which led to high and controllable nitrogen contents (4.0% to 12.0%) after pyrolysis. NG thermally treated at 900 °C shows a stable methanol cross-over effect, high current density (6.67 mA cm⁻²) and durability (~

1
2
3 87% after 10,000 cycles) when catalyzing ORR in alkaline solution. Further, iron (Fe)
4 nanoparticles could be incorporated into NG with the aid of Fe(III) chloride in the synthetic
5 process. This allows one to examine the influence of non-noble metals on the electrocatalytic
6 performance. Remarkably, we found that NG supported with 5 wt% Fe nanoparticles displayed
7 an excellent methanol cross over effect and high current density (8.20 mA cm^{-2}) in an alkaline
8 solution. Moreover, Fe incorporated NG showed almost four-electron transfer processes and
9 superior stability both in alkaline ($\sim 94\%$) and acidic ($\sim 85\%$) solutions, which outperformed the
10 platinum and NG-based catalysts.
11
12
13
14
15
16
17
18
19
20
21

22
23 **KEYWORDS:** graphene oxide, nitrogen doped graphene, iron coordination, oxygen reduction
24 reaction, stability
25
26
27

28
29 The cathodic oxygen reduction reaction (ORR) plays a crucial role in electrochemical energy
30 conversion in fuel cells.¹ Platinum based materials have long been used as active catalysts for
31 the ORR; however, these noble metal catalysts hinder widespread commercialization of fuel cells
32 due to their high cost, sluggish electron transfer kinetics and limited supply.²⁻⁴ Moreover, during
33 a long term electrochemical process, Pt-based catalysts generally suffer from surface oxide
34 formation, particle dissolution and aggregation in alkaline electrolytes.^{5,6} Therefore, numerous
35 efforts have been devoted to finding a suitable substitute for Pt-based catalysts including
36 nitrogen doped carbon nanotubes,⁷⁻⁹ mesoporous graphitic arrays¹⁰ and non-precious transition
37 metal catalysts (such as iron or cobalt coordinated to nitrogen doped carbons).^{11,12} The
38 advantages of these alternative catalysts include low cost, excellent electrocatalytic activity, long
39 durability and an environmentally benign character. In general, the transition metal catalysts can
40 be synthesized by pyrolyzing precursors containing nitrogen, Fe or Co salts and macrocyclic
41 compounds (like Co(II) or Fe(II) phthalocyanine or methoxyphenyl porphyrin) adsorbed on
42
43
44
45
46
47
48
49
50
51
52
53
54
55
56
57
58
59
60

1
2
3 carbon black (CB).¹²⁻¹⁶ However, when the pyrolysis temperature is higher than 800 °C,
4
5 gasification of CB occurs, especially in the presence of NH₃; this results in mass loss of carbon
6
7 and consequently shortens the lifespan of these catalysts.^{17,18} Although the nature of nitrogen
8
9 atoms in nitrogen doped carbon materials and the catalytically active sites in metal-nitrogen-
10
11 carbon (M-N-C) remain controversial,^{19,20} both quantum mechanical calculations²¹ and
12
13 experimental investigations²² indicate that pyridinic and/or graphitic nitrogen moieties play an
14
15 essential role in catalyzing the ORR.²³
16
17
18
19

20
21 Graphene is a monolayer of carbon atoms arranged in a two-dimensional honeycomb network. It
22
23 shows many intriguing properties such as high surface area,²⁴ excellent electrical conductivity,²⁵
24
25 and high thermal and chemical stability.²⁶ Recently, nitrogen doped graphene (NG) has been
26
27 shown to possess high electrocatalytic activity and long-term operational stability when
28
29 catalyzing the ORR.²⁷ The high surface area of NG results in many active sites for coordination
30
31 with Fe or Co, which may lead to enhanced electrochemical performance and hence improve
32
33 catalysis of the ORR. However, there are only a handful of studies on the preparation of NG
34
35 including: treating graphene in ammonia at high temperature,^{28,29} using an ammonia plasma,³⁰
36
37 and growth of NG on Ni substrates by chemical vapor deposition (CVD).²⁷ All these processes
38
39 require vacuum conditions and are difficult to scale up, which limits the practical use of NG.
40
41
42 Therefore, an expeditious method to fabricate NG with controllable nitrogen moieties and high
43
44 surface area is highly desirable.
45
46
47
48

49
50 Herein, we report the facile synthesis of NG by immobilizing graphitic carbon nitride (CN) on
51
52 graphene sheets to form a carbon nitride-graphene composite (CN-G). The CN-G composite is
53
54 then subjected to thermal treatment, leading to the decomposition of CN and thereby introducing
55
56 nitrogen moieties into graphene. In this way, NG sheets with nitrogen content from 4.0% to
57
58
59
60

1
2
3 12.0% can be obtained by controlling the pyrolysis temperature. Furthermore, NG infused with
4 iron nanoparticles (NG/Fe) can be synthesized by the addition of iron salts (*e.g.* FeCl₃) into the
5 CN-G. We show that NG containing 5 wt% Fe exhibits high electrocatalytic activity, low onset
6 potential, excellent methanol cross over effect and long-term stability in oxygen reduction
7 reactions in both acid and alkaline solutions. These traits represent clear advantages over
8 commercially available Pt-based electrodes (30 wt% Pt on Vulcan XC72).
9
10
11
12
13
14
15
16
17

18 **RESULTS AND DISCUSSION**

20
21 The synthesis of NG is illustrated in Figure 1. In the first step, graphene oxide (GO) was
22 modified by a surfactant (sodium dodecylbenzenesulfonic acid, SDBS) to enhance the dispersion
23 of GO in water. Afterwards, cyanamide (4 mL) was added dropwise into the GO (1 mg/mL)
24 solution (see Experimental section for details). The mixture was then heated to 100 °C,
25 continuously stirring, to remove water. Subsequently, the resultant solid powder was annealed at
26 550 °C under an argon flow for 4 h to trigger the thermal condensation of cyanamide, providing
27 polymeric CN.³¹ Further heat treatment of the CN-G at 800, 900 and 1000 °C gave rise to CN
28 decomposition, and thereby generated NG. For simplicity, the samples are denoted as NG-800,
29 NG-900 and NG-1000 respectively.
30
31
32
33
34
35
36
37
38
39
40
41
42

43 The morphology and structure of CN-G were first investigated by transmission electron
44 microscope (TEM) and scanning electron microscope (SEM). CN without incorporation of
45 graphene sheets shows a typical slate like morphology,³² while CN-G becomes crumpled (Figure
46 S1) due to the adsorbed cyanamide on graphene, which undergoes polymerization under thermal
47 treatment. As indicated in Figure 2a, graphene sheets were not distinctively visible in CN-G due
48 to the thick layer of CN adsorbed on graphene surface. The XRD patterns of CN, which stacks
49
50
51
52
53
54
55
56
57
58
59
60

1
2
3 like graphite with a tri-s-triazine unit, feature two diffraction peaks at around 27.2° and 13.1° .³¹
4
5 After the introduction of graphene, the unchanged XRD pattern suggests that graphene sheets are
6
7
8 homogeneously distributed in CN without disrupting their solid state packing (Figure 2b).
9

10
11 Thermogravimetric analysis (TGA) of CN-G containing 5.0 wt% of graphene reveals that weight
12
13 loss starts at around 600°C (Figure S2), which can be assigned to the decomposition of CN.
14
15 After treatment at 800°C , a total $\sim 95\%$ weight loss of the composite suggests that only
16
17
18 graphene remains. TEM images (Figure 2c and S3) of the NG-800, NG-900 and NG-1000
19
20 demonstrate transparent graphene sheets without the presence of any residual CN. A Brunauer-
21
22 Emmett-Teller (BET) surface area of $508\text{ m}^2\text{ g}^{-1}$ for NG-900 (Figure S4) is obtained, which is
23
24
25 higher than that of NG produced by other methods.^{33,34} In addition, a narrow pore-size
26
27
28 distribution centered at about 3.1 nm and a total pore volume of $3.674\text{ cm}^3\text{ g}^{-1}$, can be derived
29
30
31 from the adsorption branch of the isotherms based on the Barrett-Joyner-Halenda (BJH) model.
32

33
34 To probe the chemical composition and content of nitrogen in NG, X-ray photoelectron
35
36 spectroscopic (XPS) measurements were carried out on NG-800, NG-900 and NG-1000 (Figure
37
38
39 2d and S5). As shown in Figure 2d, the survey spectra of NG samples reveals the presence of C,
40
41
42 O, and N and a nitrogen content of 12.0, 5.0, and 4.0% in NG-800, NG-900 and NG-1000,
43
44
45 respectively. This is consistent with the values determined by elemental analysis (Figure S5).
46
47
48 Furthermore, absence of an S 2p peak at 165.0 eV (Figure S5e) indicates that the surfactant
49
50
51 (SDBS) was completely decomposed upon pyrolysis. The C 1s peaks for the NG samples (Figure
52
53
54 S6a) center at approximately 284.6 eV and are slightly asymmetric. This is a common effect for
55
56
57 nitrogen doped carbon materials.³⁵ The width of the C 1s peaks become smaller as the pyrolysis
58
59
60 temperature increases from 800 to 1000°C , suggesting enhanced graphitization at higher
temperature. This result is further supported by the Raman spectrum (Figure S7); the G band

1
2
3 becomes sharper and the intensity ratio of the G to the D band (I_G/I_D) increases.³⁶ Analysis of N
4
5
6
7
8
9
10
11
12
13
14
15
16
17
18
19
20
21
22
23
24
25
26
27
28
29
30
31
32
33
34
35
36
37
38
39
40
41
42
43
44
45
46
47
48
49
50
51
52
53
54
55
56
57
58
59
60

becomes sharper and the intensity ratio of the G to the D band (I_G/I_D) increases.³⁶ Analysis of N
1s spectra reveals the presence of pyridinic- and graphitic- nitrogen corresponding to binding
energies of 398.4 and 401.0 eV, respectively (Figure S6).²³ In addition, the reaction between
oxygen containing groups in GO and nitrogen species during the synthesis results in the
formation of pyridinic N^+-O^- at 402.0-404.0 eV.³⁷ In NG-800, pyridinic-N is more prevalent
than graphitic-N, with content of 7.92% and 3.45%, respectively (Figure 3a). Upon raising the
pyrolysis temperature to 900 and 1000 °C, the overall nitrogen content decreases dramatically.
Interestingly, the pyridinic-N content largely drops to 1.47% at 900 °C and 1.14% at 1000 °C,
whereas the graphitic-N slowly decreases. However, the content of graphitic-N is higher than
that of pyridinic-N at 900 and 1000 °C. Furthermore, the ratio of graphitic-N to pyridinic-N
content in NG-800, NG-900 and NG-1000 shows significant differences (*i.e.* 0.44, 1.73 and 1.66,
respectively). A slight increase in pyridinic N^+-O^- is observed from NG-800 to NG-900, but
remains unchanged in NG-1000. This type of nitrogen species does not significantly contribute
to the ORR performance and is unstable under fuel cell operating conditions.³⁸ Therefore, such
different amounts of nitrogen bonding configurations in NG samples is expected to play a crucial
role for the ORR electrocatalytic performances.³⁹ The X-ray diffraction (XRD) of NG samples in
Figure S8 shows a pronounced broad peak at 26.1°, attributable to the π -stacking of graphene
sheets.²⁷ The absence of a diffraction peak at 13.1° also suggests that CN is successfully
removed upon pyrolysis. The N-doping may lead to an increased interlayer spacing in NG²⁷ and
as the nitrogen content decreases from NG-800 to NG-1000, the diffraction peaks become
sharper.

The electrocatalytic activity of NG for the ORR was first examined – in a 0.1 M KOH solution
saturated with argon or oxygen – by cyclic voltammetry (CV) at a scan rate of 100 mV s⁻¹. As

1
2
3 shown in Figure 4a, featureless voltammetric currents within the potential range of -1.2 to +0.2 V
4
5 were observed for NG-900 in the argon saturated solution (dotted curve). In contrast, when the
6
7 electrolyte was saturated with O₂, a well-defined cathodic peak centered at -0.16 V was detected,
8
9 suggesting pronounced electrocatalytic activity of NG-900. A possible cross over effect in NG-
10
11 900 and Pt/C against the electrooxidation of methanol in O₂ saturated 0.1M KOH in the presence
12
13 of methanol (3.0 M) was also detected. The Pt/C shows a pair of peaks at -0.15 V and -0.08 V
14
15 corresponding to methanol oxidation, whereas the cathodic peak for the ORR disappears (Figure
16
17 4b). In contrast, no noticeable change was seen in the oxygen reduction current on NG-900 under
18
19 the same experimental conditions (Figure 4a), suggesting high selectivity and good stability of
20
21 NG-900 for the ORR with respect to Pt/C.
22
23
24
25
26

27
28 To further evaluate the electrocatalytic activity of NG, both rotating ring disk electrodes (RRDE)
29
30 and rotating disk electrodes (RDE) were employed. Figure 5a shows the steady state
31
32 voltammograms for different NG samples loaded on a glassy carbon electrode in O₂ saturated 0.1
33
34 M KOH. The corresponding ring current (I_R) for the oxidation of hydrogen peroxide ions (HO₂⁻)
35
36 was measured with a Pt ring electrode with a potential of 0.50 V. The electron transfer number
37
38 per oxygen molecule involved in the ORR of the NG-800, NG-900 and NG-1000 electrode was
39
40 calculated to be 3.35, 3.70 and 3.48, respectively. The calculation used Eq. 1⁷ and a potential of -
41
42 0.4V
43
44
45

$$n = 4I_D / (I_D + I_R/N) \quad (1)$$

46
47
48 where $N = 0.36$ is the collection efficiency, I_D is the disk current, and I_R is the ring current. The
49
50 lower ring current of NG-900 compared to NG-800 and NG-1000 suggests that a lower amount
51
52 of HO₂⁻ reached the ring electrode under increasing negative potentials. The onset potential of
53
54
55
56
57
58
59
60

1
2
3 NG-900 was determined to be -0.03 V, which is close to that identified from CV measurements
4 (-0.04 V, Figure 5a). Different from a Pt/C electrode, the NG-900 electrode showed an enhanced
5 steady-state diffusion current over a large potential range.
6
7
8
9

10
11 The current density (J_K) of the NG samples was analyzed by RDE and calculated on the basis of
12 the Koutecky-Levich equations [Eq. (2) – (4)].¹⁰
13
14

$$\frac{1}{J} = \frac{1}{J_L} + \frac{1}{J_K} = \frac{1}{B\omega^{1/2}} + \frac{1}{J_K} \quad (2)$$

$$B = 0.62nFC_0(D_0)^{2/3}\nu^{-1/6} \quad (3)$$

$$J_K = nFkC_0 \quad (4)$$

15
16
17
18
19
20
21 where J is the measured current density, J_K and J_L are the kinetic and diffusion limiting current
22 densities, ω is the angular velocity of the disk ($\omega = 2\pi N$, N is the linear rotation speed), n is the
23 overall number of electrons transferred in the oxygen reduction, F is the Faraday constant (96485
24 C mol⁻¹), C_0 is the bulk concentration of O₂, ν is the kinematic viscosity of the electrolyte, and k
25 is the electron transfer rate constant. The Koutecky-Levich plot of J^{-1} vs. $\omega^{-1/2}$ at a potential of -
26 0.40 V on the NG-900 electrode exhibited good linearity (Figure 5c). As shown in Figure 5d, the
27 calculated J_K value of 6.67 mA cm⁻² at -0.40 V is much higher than that of Pt/C (4.76 mA cm⁻² at
28 -0.40 V), and is comparable or even higher than previous reports on nitrogen doped graphene,
29 CNTs, and other types of carbon materials.^{27,29,40,41} In association with the XPS and
30 electrochemical results described for NG-800, NG-900 and NG-1000, the content of pyridinic-N
31 among the different nitrogen species does not play a significant role in the performance of the
32 ORR. In contrast, the electrochemical performance is dependent on the content of graphitic-N,
33
34
35
36
37
38
39
40
41
42
43
44
45
46
47
48
49
50
51
52
53
54
55
56
57
58
59
60

1
2
3 for which a higher ratio of graphitic-N over pyridinic-N in NG-900 than NG-800 and NG-1000
4
5 might be responsible for the high catalytic performance.¹⁰
6
7

8
9 It has been reported that the pyridinic nitrogen enriched carbon material can be favorable for the
10
11 fabrication of Fe-N-C based catalysts.⁴² Given that the present synthetic approach offers a high
12
13 content of pyridinic-N sites in the CN-G composite, one can expect that the introduction of Fe
14
15 salts to CN-G will lead to an incorporation of Fe nanoparticles into NG and provide efficient
16
17 coordination between Fe and pyridinic-N. Towards this end, NG decorated with Fe nanoparticles
18
19 was prepared by mixing FeCl₃ with the precursors GO and cyanamide, followed by subsequent
20
21 thermal treatment at 900 °C (Figure S9). The detailed procedure can be found in the
22
23 experimental section. NG samples with different Fe content were prepared in this work and are
24
25 denoted as NG/Fe_x (where x = 2.0, 5.0, 10.0 and 15.0 wt%).
26
27
28
29
30

31 Figure 6a shows the XRD pattern of NG/Fe_{5.0}. The diffraction peak at 42.8° is characteristic for
32
33 Fe (110). In addition, HRTEM images display the presence of small (2-4 nm) crystalline Fe
34
35 nanoparticles on NG. They also show a lattice d-spacing of ~ 0.23nm, which is slightly higher
36
37 than the standard value of 0.203 nm (JCPDS database) (Figure 6b and c). The larger d-spacing
38
39 might be attributed to Fe nanoparticles incorporated into the nitrogen lattice, which enlarges the
40
41 lattice constant.⁴³ The presence of N and Fe in the composite can be further validated by the
42
43 corresponding energy dispersive X-ray (EDX) analysis (Figure 6d). Increasing the Fe content to
44
45 15.0 wt% (*i.e.* NG/Fe_{15.0}) results in the agglomeration of ~ 50 nm Fe nanoparticles. In contrast,
46
47 no large nanoparticles were visible in NG/Fe_{5.0} (Figure S10a,b). The XPS survey spectra of
48
49 NG/Fe_{5.0} shows the presence of Fe 2p and Fe 3p, in addition to N 1s, C 1s and O 1s peaks
50
51 (Figure S11). Unfortunately, the Fe 3p peak (~ 52-56 eV) is too weak to determine the valence
52
53 state of Fe.
54
55
56
57
58
59
60

1
2
3 The catalytic properties of NG/Fe_x samples were first assessed with cyclic voltammetry in a 0.1
4 M KOH solution. The NG/Fe_{5.0} shows a featureless voltammetric current within the potential
5 range of -1.2 to +0.2 V in an Ar-saturated alkaline solution (Figure S12). Saturating the
6 electrolyte with O₂ results in a well-defined cathodic peak at ~ 0.20 V. Similar to NG-900,
7 NG/Fe_{5.0} did not show any change in the oxygen reduction current in an O₂ saturated alkaline
8 solution in the presence of 3.0 M methanol, making the catalyst very stable against crossover
9 effects. However, two additional peaks were observed at -0.61 and -0.93 V, which are associated
10 with the redox reaction of the iron nanoparticles.⁷ Figure 7a shows the RRDE polarization curves
11 of NG/Fe_x composites supported on a glassy carbon electrode in O₂ saturated 0.1 M KOH. The
12 electron transfer number for NG/Fe_x samples, at the potential of -0.4 V, was calculated to be
13 3.79, 3.91, 3.80 and 3.79 for the NG/Fe_{2.0}, NG/Fe_{5.0}, NG/Fe_{10.0} and NG/Fe_{15.0}, respectively. All
14 samples of NG loaded with Fe nanoparticles greatly enhanced the electrochemical performance
15 leading to four electron transfer processes in the ORR. Although the onset potential for the ORR
16 at the NG/Fe_{5.0} electrode was similar (*i.e.* -0.04 V) to that of Pt/C, the reduction current was
17 significantly higher (Figure S12). As shown in Figure 7b, the calculated current density (J_K)
18 value of NG/Fe_{2.0}, NG/Fe_{5.0}, NG/Fe_{10.0} and NG/Fe_{15.0} is 3.57, 8.20, 7.69 and 5.26 mA cm⁻²,
19 respectively. This result suggests that increasing the Fe content leads to an increase in the
20 concentration of active catalytic sites until all pyridinic-N is coordinated (at 5.0 wt%).⁴⁴
21 Increasing the Fe content from 5.0 wt% to 10.0 and 15.0 wt% produces uncoordinated metal
22 particles (Figure S10) which do not provide additional catalytic sites.⁴⁵ Therefore, no
23 enhancement of the current density or electron transfer number was observed for NG/Fe_{10.0} and
24 NG/Fe_{15.0}. It is remarkable to note that NG/Fe_{5.0} has a current density almost two times higher
25 than Pt/C (4.76 mA cm⁻²). This suggests that incorporating Fe nanoparticles into NG provides a
26
27
28
29
30
31
32
33
34
35
36
37
38
39
40
41
42
43
44
45
46
47
48
49
50
51
52
53
54
55
56
57
58
59
60

1
2
3 synergistic coupling between Fe and NG that results in an outstanding electrocatalytic
4 performance compared to Pt/C and NG-900.
5
6

7
8
9 Another set of NG/Fe_x samples were prepared by treatment at 800 °C and 1000 °C. Figure S14
10 shows the summarized results of electron transfer number and J_K values obtained from both
11 RRDE and RDE. The catalytic performance of NG/Fe_{5.0} (at 800 °C) is lower than that of the
12 samples prepared at 900 °C (Figure S13a). Surprisingly, NG/Fe_{5.0} prepared at 1000 °C (Figure
13 S14b) showed a higher electron transfer number and J_K than samples prepared at 800 °C and
14 slightly lower values than NG/Fe_{5.0} prepared at 900 °C. This result suggests that the oxygen
15 reduction reaction rate increases with heat-treatment temperature of the catalysts, reaching a
16 plateau at < 1000 °C.^{46,47} Thus, it can be concluded that the higher content of pyridinic-N alone
17 (by lower temperature treatment) does not necessarily result in high catalytic performance. In
18 addition, the temperature for catalyst preparation plays an important role in the synergistic
19 coupling between Fe and nitrogen components in the composites.
20
21
22
23
24
25
26
27
28
29
30
31
32
33
34

35
36 Furthermore, NG/Fe_x composites also showed high ORR activity in acidic solution. Both RRDE
37 and RDE measurements were carried out in 0.5 M H₂SO₄ solution (Figure 7c and d). All the NG
38 samples containing Fe again showed higher electron transfer numbers compared to NG samples
39 at the potential of 0.2V vs. Ag/AgCl. At 1600 rpm, the NG/Fe_{5.0} showed a maximum J_K of about
40 1.47 mAcm⁻² with almost four-electron transfer ($n= 3.82$) processes and the lowest onset
41 potential (0.47V vs. Ag/AgCl) of all tested electrodes. The catalytic activity order of the NG/Fe_x
42 catalysts in acidic medium was the same as that in alkaline medium, but they showed much
43 higher current density in the alkaline solution.
44
45
46
47
48
49
50
51
52
53
54
55
56
57
58
59
60

1
2
3 To examine the influence of any un-coordinated Fe nanoparticles (*i.e.* Fe residues) in the NG/Fe_x
4 composites on the electrocatalytic performance, NG/Fe_{5.0} was first treated in 2M H₂SO₄ at 80 °C
5
6 for 3 h and again subjected to ORR measurements in alkaline and acidic solutions. Remarkably,
7
8 the acid treated NG/Fe_{5.0} showed almost same ORR catalytic activity and a similar onset
9
10 potential, electron transfer number, and current density in both acidic and alkaline media (Figure
11
12 8). This result shows that Fe residues do not significantly contribute to the ORR performance.
13
14
15
16
17

18 The stability of NG-900, NG/Fe_{5.0}, and Pt/C electrodes toward the ORR was first examined by
19
20 continuous potential cycling between +0.2 to -1.2 V in O₂ saturated 0.1M KOH for 10,000 cycles
21
22 (Figure S13). As indicated in Figure S15a, the deterioration of the Pt/C electrode resulted in a ~
23
24 58% drop in current density. In contrast, NG-900 and NG/Fe_{5.0} electrodes showed only a slight
25
26 decay of current density – ~ 13% and ~ 6% at -0.15 V, respectively (Figure S15b and c). The
27
28 voltammetric response of the two electrodes also remained unchanged after the continuous
29
30 potential cycles. In addition, the NG/Fe_{5.0} showed only ~ 15% decay in the current density (at
31
32 0.38V) in acidic medium after 10,000 cycles (Figure S12d). These results show that NG/Fe_{5.0}
33
34 exhibited superior durability over Pt/C based catalysts.
35
36
37
38
39

40 CONCLUSION

41
42
43 In summary, we report a facile and scalable method to prepare NG to catalyze the ORR in a fuel
44
45 cell. The prominent features of synthesized the NG include high nitrogen content, high surface
46
47 area, high electrocatalytic activity, and superior durability. The incorporation of Fe nanoparticles
48
49 into the NG results in significantly enhanced performance of graphene based catalysts. These
50
51 NG/F_x catalysts feature the almost four electron transfer processes, high current density, and
52
53 superb stability. They also outperform Pt/C towards ORR in both in acidic and alkaline media. In
54
55
56
57
58
59
60

1
2
3 addition to their promising application as fuel cell catalysts, we anticipate that NG with and
4
5 without metal nanoparticles will provide broad applications in the field of lithium ion batteries,
6
7 sensors, field-effect transistors and supercapacitors.
8
9

10 11 **Experimental Section**

12
13
14
15 **Synthesis of GO, NG and NG/Fe_x composites:** Graphite oxide was prepared from natural
16
17 graphite by a modified Hummers' method.⁴⁸ Graphene-carbon nitride (G-CN) composites were
18
19 prepared by electrostatic interaction between anionic surfactant modified graphene oxide (GO)
20
21 and cyanamide precursor for synthesizing carbon nitride (CN). In a typical synthesis, 0.1g of the
22
23 surfactant sodium dodecylbenzene sulfonic acid (SDBS) was mixed with 100 mL of GO
24
25 dispersion (1 mg/mL) in water and sonicated for 30 min. Then, 4 mL of cyanamide solution (50
26
27 wt% in water) was added dropwise. The mixture was then stirred continuously and heated at 100
28
29 °C to remove water. The resulting solid was calcined in two different steps. In the first step, the
30
31 solid products were heated to 550 °C at a rate of 2 °C/min and tempered at this temperature for
32
33 another 4 h to form CN.³¹ To prepare NG, the resulting CN-G composites were further heated to
34
35 800, 900 and 1000 °C. All the sample annealing and cooling processes were carried out under
36
37 argon flow. For comparison, undoped and reduced GO (rGO) was also prepared by pyrolyzing
38
39 pure GO under the same annealing processes.
40
41
42
43
44
45

46
47 Composites of NG with iron nanoparticles were synthesized by adding the desired amount (*i.e.* 2,
48
49 5, 10 and 15 mg) of FeCl₃ to 100 mg of GO solution (1 mg/mL) and sonicating the mixture for 1
50
51 h. The content of Fe (*i.e.* 2.0, 5.0, 10.0 and 15.0 wt%) in the composites was calculated with
52
53 respect to the total mass of GO into the solution. Then 4 mL of cyanamide solution was added
54
55 dropwise. The reaction mixture was then heated at 100 °C with continuous stirring to remove
56
57
58
59
60

1
2
3 water. The resulting solid was then calcined at 550 °C for 4 h to form CN and then pyrolysed
4
5 separately at 800, 900 and 1000 °C for 1 hr to decompose the CN. All the annealing processes
6
7 were carried under argon atmosphere.
8
9

10
11 **Characterization:** The morphology and microstructures of the samples were investigated by
12
13 HRTEM (Philips Tecnai F20), TGA (Mettler TG 50), XRD (Bruker D4 X-ray scattering system
14
15 with Ni filtered Cu K α radiation). Raman spectra were recorded with a Bruker RFS 100/S
16
17 spectrometer. Nitrogen sorption isotherms and BET surface areas were measured at 77 K with a
18
19 Micromeritics Tristar 3000 analyzer (USA). The chemical composition was analyzed by XPS
20
21 with an Omicron Multiprobe spectrometer using Al K α radiation. For these measurements CN-G
22
23 composites were ultrasonicated in ethanol and then casted and dried at ambient conditions on Au
24
25 substrates (30 nm Au films thermally evaporated on Cr-primed Si wafers, Georg-Albert PVD-
26
27 Coatings). XPS binding energies were referenced to the Au 4f $_{7/2}$ peak (84.0 eV). Elemental
28
29 chemical ratios in CN-G composites were calculated from areas of the XP peaks. The
30
31 calculations assumed a homogeneous distribution of elements in the samples and normalized the
32
33 peak areas with Scofield sensitivity factors and electron attenuations lengths evaluated from the
34
35 Laibinis expression. For the analysis of N1s spectra a Shirley background subtraction procedure
36
37 was employed and symmetric Voigt functions (90 % of Gaussian character) were used for fitting.
38
39 All fits were self-consistent.
40
41
42
43
44
45

46
47 **Electrocatalytic activity evaluation:** The ORR activity and four-electron selectivity of the
48
49 nitrogen doped graphene samples were evaluated using a rotating disk electrode (RDE) and a
50
51 rotating ring disk electrode (RRDE), respectively. RDE/RRDE measurements were performed
52
53 using CHI Electrochemical Station (Model 760D) in a conventional three-electrode
54
55 electrochemical cell. Platinum wire and an Ag/AgCl, KCl (3M) electrode were used as the
56
57
58
59
60

1
2
3 counter and reference electrode, respectively. The preparation of a glassy carbon working
4 electrode (5 mm in diameter) is as follows: prior to use the working electrode was polished
5 mechanically with 0.05 μm alumina slurry to obtain a mirror like surface, then washed with Mill-
6 Q water and acetone and allowed to dry. 1 mg of the prepared NG sample was dissolved in a 1
7 mL solvent mixture of Nafion (5 wt%) and water (V:V ratio = 1:9) using sonication. For
8 comparison, a commercially available catalyst of 30 wt% Pt supported on black carbon (fuel cell
9 grade) was used and a 1 mg/mL Pt/C suspension was prepared according to the same procedure
10 described above. The electrodes were allowed to dry at room temperature before the
11 measurement. This leads to a catalyst (NG samples or Pt/C) loading of $50.91 \mu\text{g cm}^{-2}$.
12
13
14
15
16
17
18
19
20
21
22
23
24

25 The RRDE experiments were carried out in an O_2 saturated 0.1 M KOH solution. The potential
26 was varied from +0.2 to -1.2 V at a potential sweep of 10 mVs^{-1} ; the ring potential was set to 0.5
27 V. First, the potential range was cyclically scanned between -1.2 and +0.2 V at a scan rate of 100
28 mV s^{-1} at ambient temperature after purging with O_2 or Ar gas for 15 min. Then the RRDE
29 experiments were performed. RRDE experiments in acidic conditions were performed in an O_2 -
30 saturated 0.5M H_2SO_4 solution within the potential range of + 0.8 to -0.2V at a potential sweep
31 of 10 mVs^{-1} and a ring potential of 1.0 V.
32
33
34
35
36
37
38
39
40
41
42

43 *Acknowledgement:* This work was financially supported by the Max Planck Society through the
44 program ENERCHEM, DFG Priority Program SPP 1459, BMBF LiBZ Project, BMBF
45 Graphenoid project, ESF Project GOSPEL (Ref Nr: 09-EuroGRAPHENE-FP-001), EU Project
46 GENIUS and ERC grant on NANOGRAPH.
47
48
49
50
51
52

53 *Supporting Information Available:* SEM, TGA of CN and CN-G samples; HRTEM, BET, XPS
54 of C1s, N1s and S 2p spectra, Raman characterizations of NG; synthetic scheme, TEM, XPS
55
56
57
58
59
60

1
2
3 spectra and electrochemical characterizations of NG/Fe_x samples. This material is available free
4 of charge *via* the Internet at <http://pubs.acs.org>.
5
6
7

8 REFERENCES

- 9
10
11 1. Steele, B.C.H.; Heinzl, A. Materials for Fuel-Cell Technologies. *Nature* **2001**, *414*, 345-352.
12
13 2. Shao, Y.Y.; Liu, J.; Wang, Y.; Lin, Y.H. Novel Catalyst Support Materials for PEM Fuel
14 Cells: Current Status and Future Prospects. *J. Mater Chem.* **2009**, *19*, 46-59.
15
16 3. Chen, W.; Chen, S.W. Oxygen Electroreduction Catalyzed by Gold Nanoclusters: Strong
17 Core Size Effects. *Angew. Chem. Int. Ed.* **2009**, *48*, 4386-4389.
18
19 4. Chen, W.; Kim, J.M.; Sun, S.H.; Chen, S.W. Electrocatalytic Reduction of Oxygen by FePt
20 Alloy Nanoparticles. *J. Phys. Chem. C* **2008**, *112*, 3891-3898.
21
22 5. Gewirth, A.A.; Thorum, M.S. Electroreduction of Dioxygen for Fuel-Cell Applications:
23 Materials and Challenges. *Inorg. Chem.* **2010**, *49*, 3557-3566.
24
25 6. Jin, W.; Du, H.; Zheng, S.L.; Xu, H.B.; Zhang, Y. Comparison of the Oxygen Reduction
26 Reaction between NaOH and KOH Solutions on a Pt electrode: The Electrolyte-Dependent
27 Effect. *J. Phys. Chem. B* **2010**, *114*, 6542-6548.
28
29 7. Gong, K.P.; Du, F.; Xia, Z.H.; Durstock, M.; Dai, L.M. Nitrogen-Doped Carbon Nanotube
30 Arrays with High Electrocatalytic Activity for Oxygen Reduction Reaction. *Science* **2009**,
31 *323*, 760-764.
32
33 8. Yu, D.; Zhang, Q.; Dai, L. Highly Efficient Metal-Free Growth of Nitrogen-Doped Single-
34 Walled Carbon Nanotubes on Plasma-Etched Substrates for Oxygen Reduction. *J. Am. Chem.*
35 *Soc.* **2010**, *132*, 15127-15129.
36
37
38
39
40
41
42
43
44
45
46
47
48
49
50
51
52
53
54
55
56
57
58
59
60

- 1
2
3 9. Feng, L.; Yan, Y.; Chen, Y.; Wang, L. Nitrogen-Doped Carbon Nanotubes as Efficient and
4
5 Durable Metal-free Cathodic Catalysts for Oxygen Reduction in Microbial Fuel Cells. *Energy*
6
7 *Environ. Sci.* **2011**, *4*, 1892-1899.
- 8
9
10 10. Liu, R.; Wu, D.Q.; Feng, X.; Müllen, K. Nitrogen-Doped Ordered Mesoporous Graphitic
11
12 Arrays with High Electrocatalytic Activity for Oxygen Reduction. *Angew. Chem Int. Ed.*
13
14 **2010**, *49*, 2565-2569.
- 15
16
17 11. Lefèvre, M.; Proietti, E.; Jaouen, F.; Dodelet, J.P. Iron-Based Catalysts with Improved
18
19 Oxygen Reduction Activity in Polymer Electrolyte Fuel Cells. *Science* **2009**, *324*, 71-74.
- 20
21
22 12. Wu, G.; More, K.L.; Johnston, C.M.; Zelenay, P. High-Performance Electrocatalysts for
23
24 Oxygen Reduction Derived from Polyaniline, Iron, and Cobalt. *Science* **2011**, *332*, 443-447.
- 25
26
27 13. Jasinski, R. A New Fuel Cell Cathode Catalyst. *Nature* **1964**, *201*, 1212-1213.
- 28
29
30 14. Gupta, S.; Tyrk, D.; Bae, I.; Aldred, W.; Yeager, E. Heat-Treated Polyacrylonitrile-Based
31
32 Catalysts for Oxygen electroreduction. *J. Appl. Electrochem.* **1989**, *19*, 19-27.
- 33
34
35 15. Schulenburg, H.; Stankov, S.; Schünemann, V.; Tributsch, H. Catalysts for Oxygen
36
37 Reduction From Heat-Treated Iron (III) tetramethoxyphenylporphyrin chloride: Structure and
38
39 Stability of Active Sites. *J. Phys. Chem. B* **2003**, *107*, 9034-9041.
- 40
41
42 16. Li, W.; Yu, A.; Higgins, D.C.; Llanos, B.G.; Chem, Z. Biologically Inspired Highly Durable
43
44 Iron Phthalocyanine Catalysts for Oxygen Reduction Reaction in Polymer Electrolyte
45
46 Membrane Fuel Cells. *J. Am. Chem. Soc.* **2010**, *132*, 17056-17058.
- 47
48
49 17. Jaouen, F.; Lafèvre, M.; Dodelet, J.P.; Cai, M. Heat-treated Fe/N/C Catalysts for O₂
50
51 Electroreduction: Are Active Sites Hosted in Micropores? *J. Phys. Chem. B* **2006**, *110*, 5553-
52
53 5558.
- 54
55
56
57
58
59
60

- 1
2
3
4
5
6
7
8
9
10
11
12
13
14
15
16
17
18
19
20
21
22
23
24
25
26
27
28
29
30
31
32
33
34
35
36
37
38
39
40
41
42
43
44
45
46
47
48
49
50
51
52
53
54
55
56
57
58
59
60
18. Lafèvre, M.; Dodelet, J.P. Fe-Based Electrocatalysts Made with Microporous Pristine Carbon Black Support for the Reduction of Oxygen in PEM Fuel Cells. *Electrochim. Acta* **2008**, *53*, 8269-8276.
 19. Shao, Y.Y.; Sui, J.H.; Yin, G.P.; Gao, Y.Z. Nitrogen-Doped Carbon Nanostructures and Their Composites as Catalytic Materials for Proton Exchange Membrane Fuel Cells. *Appl. Catal. B* **2008**, *79*, 89-99.
 20. Thorum, M.S.; Hankett, J.M.; Gewirth, A.A. Poisoning the Oxygen Reduction Reaction on Carbon-Supported Fe and Cu Electrocatalysts: Evidence for Metal-Centered Activity. *J. Phys. Chem. Lett.* **2011**, *2*, 295-298.
 21. Ikeda, T.; Boero, M.; Haung, S.F.; Terakura, K.; Oshima, M.; Ozaki, J. Carbon Alloy Catalysts: Active Sites for Oxygen Reduction Reaction. *J. Phys. Chem. C* **2008**, *112*, 14706-14709.
 22. Liu, G.; Li, X.G.; Ganesan, P.; Popov, B.N. Studies of Oxygen Reduction Reaction Active Sites and Stability of Nitrogen-Modified Carbon Composites for PEM Fuel Cells. *Electrochim. Acta* **2010**, *55*, 2853-2858.
 23. Yang, S.; Feng, X.; Wang, X.; Müllen, K. Graphene-Based Carbon Nitride Nanosheets as Efficient Metal-Free Electrocatalysts for Oxygen Reduction Reactions. *Angew. Chem. Int. Ed.* **2011**, *50*, 5339-5343.
 24. Stoller, M.D.; Park, S.J.; Zhu, Y.W.; An, J.H.; Rouff, R.S. Graphene-Based Ultracapacitors. *Nano Lett.* **2008**, *8*, 3498-3502.
 25. Yang, S.; Feng, X.; Ivanovici, S.; Müllen, K. Fabrication of Graphene-Encapsulated Oxide Nanoparticles: Towards High-Performance Anode Materials for Lithium Storage. *Angew. Chem. Int. Ed.* **2010**, *49*, 8408-8411.

- 1
2
3
4
5
6
7
8
9
10
11
12
13
14
15
16
17
18
19
20
21
22
23
24
25
26
27
28
29
30
31
32
33
34
35
36
37
38
39
40
41
42
43
44
45
46
47
48
49
50
51
52
53
54
55
56
57
58
59
60
26. Balandin, A.A.; Ghosh, S.; Bao, W.Z.; Calizo, I.; Teweldebrhan, D.; Miao, F.; Lau, C.N. Superior Thermal Conductivity of Single-Layer Graphene. *Nano Lett.* **2008**, *8*, 902-907.
27. Qu, L.; Liu, Y.; Baek, J.-B.; Dai, L. Nitrogen-Doped Graphene as Efficient Metal-Free Electrocatalysts for Oxygen Reduction Reaction in Fuel Cells. *ACS Nano* **2010**, *4*, 1321-1326.
28. Li, X.; Wang, H.; Robinson, J.T.; Sanchez, H.; Diankov, G.; Dai, H. Simultaneous Nitrogen Doping and Reduction of Graphene Oxide. *J. Am. Chem. Soc.* **2009**, *131*, 15939-15944.
29. Geng, D.; Chen, Y.; Chen, Y.; Li, Y.; Li, R.; Sun, X.; Ye, S.; Knights, S. High Oxygen-Reduction Activity and Durability of Nitrogen-Doped Graphene. *Energy Environ. Sci.* **2011**, *4*, 760-764.
30. Lin, Y.-C.; Lin, C.-Y.; Chiu, P.-W. Controllable Graphene N-Doping with Ammonia Plasma. *Appl. Phys. Lett.* **2010**, *96*, 133110.
31. Wang, X.C.; Maeda, K.; Thomas, A.; Takahabe, K.; Xin, G.; Carlsson, J.M.; Domen, K.; Antonietti, M. A Metal-Free Polymeric Photocatalysts for Hydrogen Production From Water Under Visible Light. *Nature Mater.* **2009**, *8*, 76-80.
32. Zhang, Y.; Thomas, A.; Antonietti, M.; Wang, X. Activation of Carbon Nitride Solids by Protonation: Morphology Changes, Enhances Ionic Conductivity and Photoreduction Experiments. *J. Am. Chem. Soc.* **2009**, *131*, 50-51.
33. Lee, K.R.; Lee, K.U.; Lee, J.W.; Ahn, B.T.; Woo, S.I. Electrochemical Oxygen Reduction on Nitrogen Doped Graphene Sheets in Acid Media. *Electrochem. Commun.* **2010**, *12*, 1052-1055.
34. Sheng, Z.H.; Shao, L.; Chen, J.J.; Bao, W.J.; Wang, F.B.; Xia, X.H. Catalyst-Free Synthesis of Nitrogen-Doped Graphene *via* Thermal Annealing Graphite Oxide with Melamine and Its excellent Electrocatalysis. *ACS Nano* **2011**, *5*, 4350-4358.

- 1
2
3
4
5
6
7
8
9
10
11
12
13
14
15
16
17
18
19
20
21
22
23
24
25
26
27
28
29
30
31
32
33
34
35
36
37
38
39
40
41
42
43
44
45
46
47
48
49
50
51
52
53
54
55
56
57
58
59
60
35. Côté, R.; Lalande, G.; Guay, D.; Dodclot, J.P.; Dénés, G. Influence of Nitrogen-Containing Precursors on the Electrocatalytic Activity of Heat-Treated Fe(OH)₂ on Carbon Black for O₂ Reduction. *J. Electrochem. Soc.* **1998**, *145*, 2411-2418.
36. Kim, T.W.; Park, I.S.; Ryoo, R.; A Synthetic Route to Ordered Mesoporous Carbon with Graphitic Pore Walls. *Angew. Chem. Int. Ed.* **2003**, *42*, 4375-4379.
37. Chen, Z.; Higgins, D.; Tao, H.; Hsu, R.S.; Chen, Z. Highly Active Nitrogen-Doped Carbon Nanotubes for Oxygen Reduction Reaction in Fuel Cell Application. *J. Phys. Chem. C* **2009**, *113*, 21008-21013.
38. Liu, G.; Li, X.; Lee, J.W.; Popov, B.N. A Review of the Development of Nitrogen-Modified Carbon-Based Catalysts for Oxygen Reduction as USC. *Catal. Sci. Technol.* **2011**, *1*, 207-217.
39. Rao, C.V.; Caberea, C.R.; Ishikawa, Y. In Search of the Active Site in Nitrogen-Doped Carbon Nanotube Electrodes for the Oxygen Reduction Reaction. *J. Phys. Chem. Lett.* **2010**, *1*, 2622-2627.
40. Jeon, I.Y.; Yu, D.; Bae, S.Y.; Choi, H.J.; Chang, D.W.; Dai, L.; Baek, J.B. Formation of Large-Area Nitrogen-Doped Graphene Film Prepared from Simple Solution Casting of Edge-Selectively Functionalized Graphite and Its Electrocatalytic Activity. *Chem. Mater.* **2011**, *23*, 3987-3992.
41. Mo, Z.; Liao, S.; Zheng, Y.; Fu, Z. Preparation of nitrogen-doped carbon nanotube arrays and their catalysis towards cathodic oxygen reduction in acidic and alkaline media. *Carbon* **2012**, *50*, 2620.

- 1
2
3
4
5
6
7
8
9
10
11
12
13
14
15
16
17
18
19
20
21
22
23
24
25
26
27
28
29
30
31
32
33
34
35
36
37
38
39
40
41
42
43
44
45
46
47
48
49
50
51
52
53
54
55
56
57
58
59
60
42. Kothandaraman, R.; Nallathambi, V.; Artyushkova, K.; Barton, S.C. Non-Precious Oxygen Reduction Catalysts Prepared by High-Pressure Pyrolysis for Low-Temperature Fuel Cell. *Appl. Catal. B* **2009**, *92*, 209-216.
43. Herzog, B.; Herein, D.; Schlögl, R. *In situ* X-ray Powder Diffraction Analysis of the Microstructure of Activated Iron Catalysts for Ammonia Synthesis. *Appl. Catal. A: General* **1996**, *141*, 71-104.
44. Lafèvre, M.; Dodelet, J.P.; Bertrand, P. Molecular Oxygen Reduction in PEM Fuel Cells: Evidence for the Simultaneous Presence of Two Active Sites in Fe-Based Catalysts. *J. Phys. Chem. B* **2002**, *106*, 8705-8713.
45. Bailey, L.D.; Trudeau, M.; Joly, A.; Schulz, R.; Lalande, G.; Guay, D.; Dodelet, J.P.; Graphitization and Particles Size Analysis of Pyrolyzed Cobalt Phthalocyanine/Carbon Catalysts for Oxygen Reduction in Fuel Cells. *J. Mater. Res.* **1994**, *9*, 3202-3209.
46. Gojković, S.Lj; Gupta, S; Savinell, R.F.; Heat-Treated Iron(III) Tetramethoxyphenyl Porphyrin Chloride Supported on High-Area Carbon as an Electrocatalysts for Oxygen Reduction. *J. Electroanal. Chem.* **1999**, *462*, 63-72.
47. Subramanian, N.P.; Li, X; Nallathambi, V; Kumaraguru, S.W.; Mercado, H.C.; Wu, G.; Lee, J.W.; Popov, B.N.; Nitrogen-Modified Carbon-Based Catalysts for Oxygen Reduction Reaction in Polymer Electrolyte Membrane Fuel Cells. *J. Power Sources* **2009**, *188*, 38-44.
48. Hummers, W,S; Offeman,R.E.; Preparation of Graphitic Oxide. *J. Am. Chem. Soc.* **1958**, *80*, 1339.

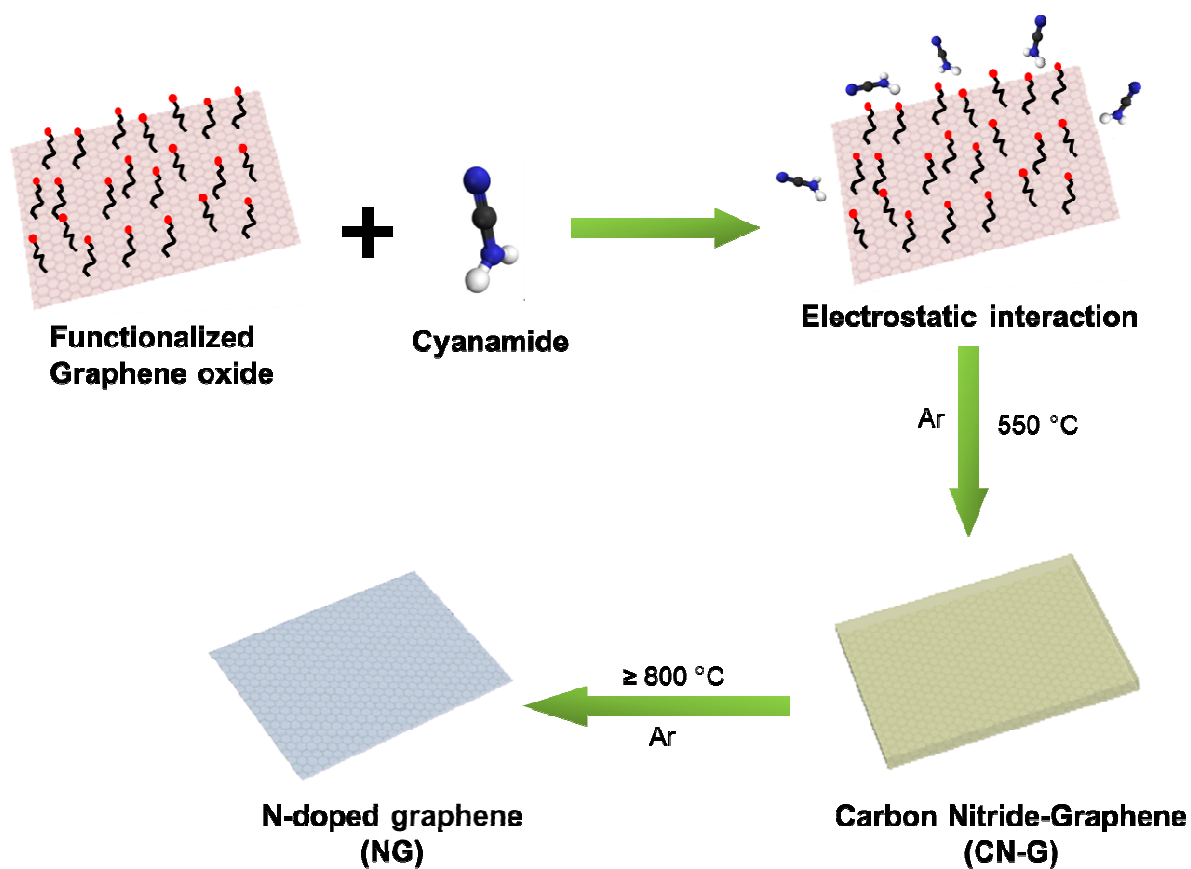


Figure 1: Preparation of NG for ORR.

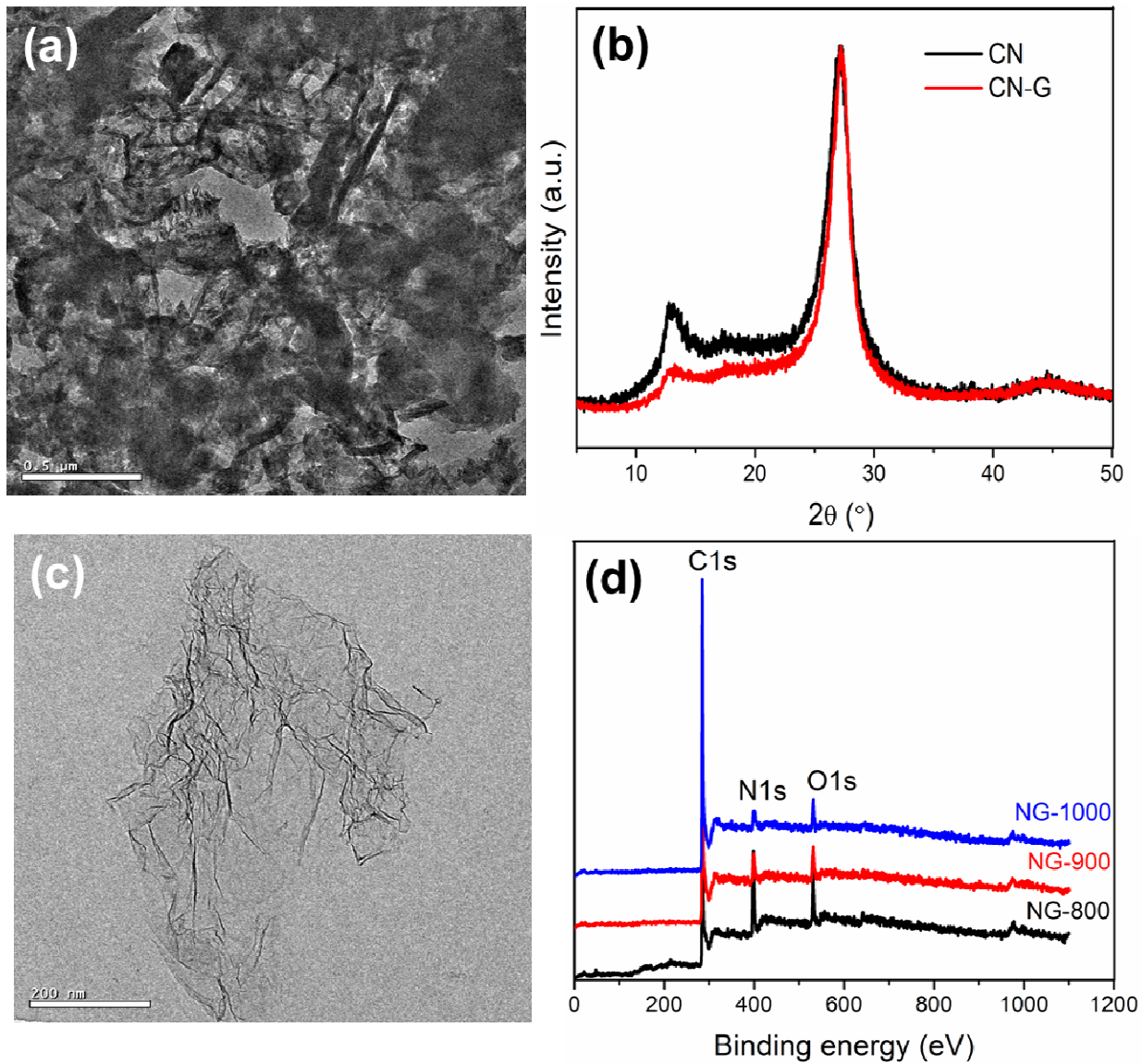


Figure 2: (a) TEM image and (b) XRD pattern of CN and CN-G composite, (c) TEM image of CN-G composite after pyrolyzing at 900 °C (*i.e.* NG-900) and (d) XPS survey of NG samples

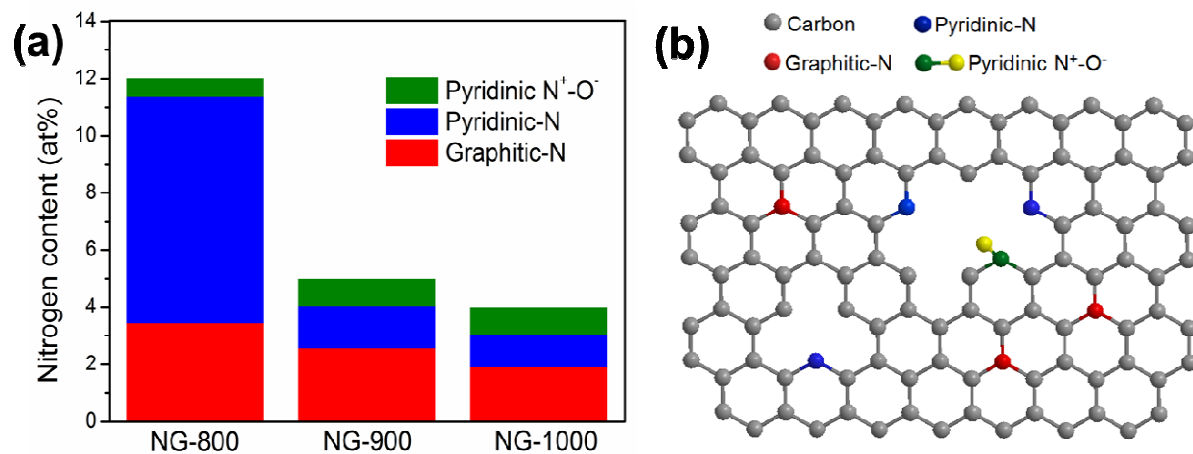


Figure 3: (a) The content of three types of nitrogen in NG, (b) Schematic representation of NG.

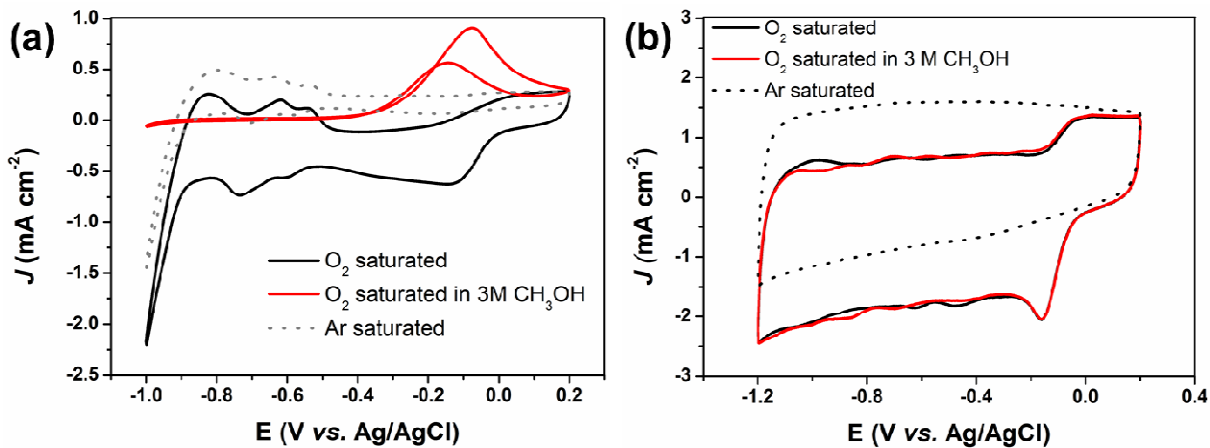


Figure 4: Cyclic voltammograms of (a) NG-900 and (b) Pt/C at a scan rate of 100 mV cm⁻¹ in O₂ or Ar-saturated 0.1M KOH solutions as well as O₂-saturated 0.1M KOH solution with 3M CH₃OH.

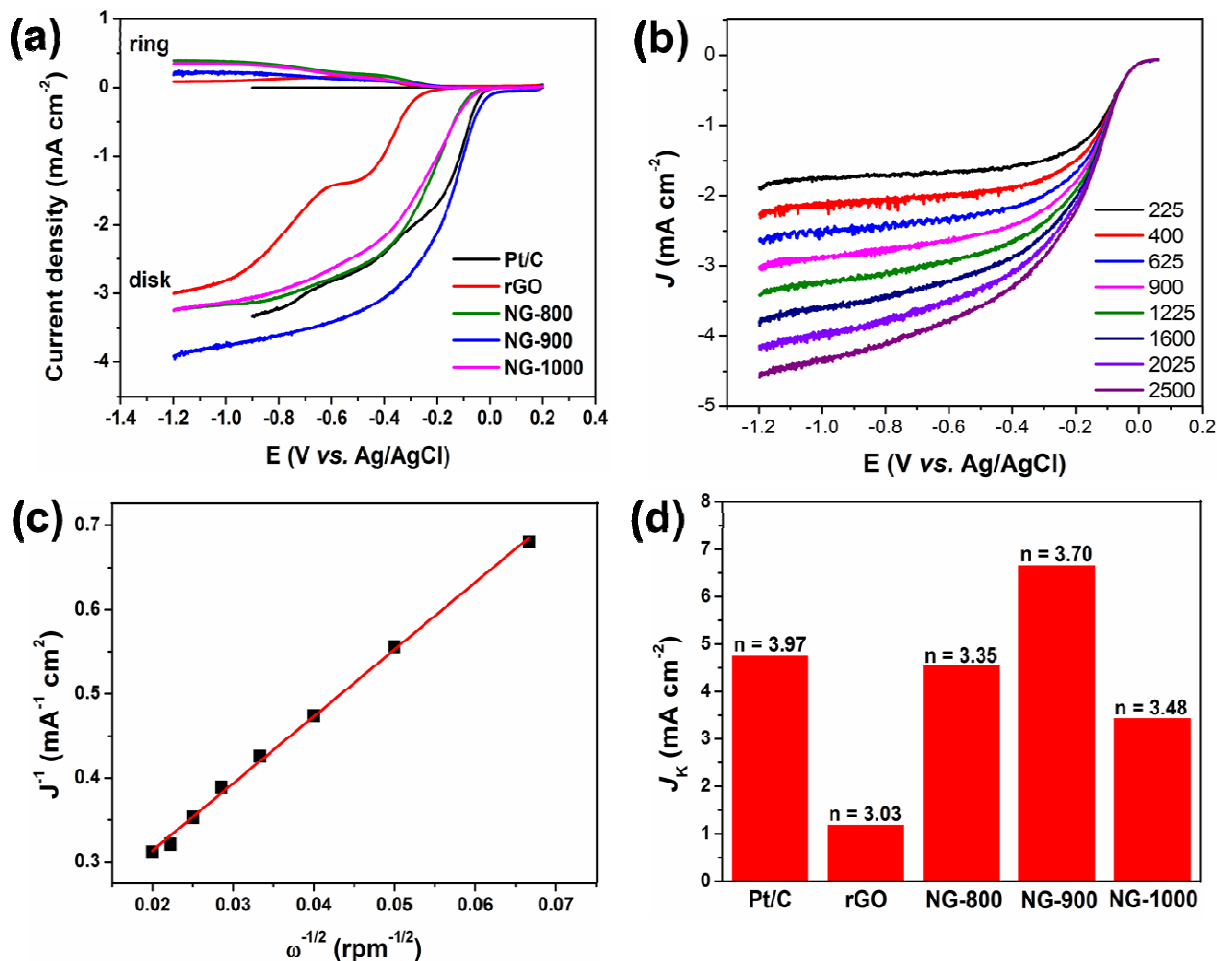


Figure 5: (a) RRDE voltammetric response for the ORR in O_2 saturated 0.1M KOH at a scan rate of 10 mVs^{-1} . The electrode rotation rate was 1600 rpm and the Pt ring electrode was polarized at 0.5 V; (b) RDE voltammograms recorded for NG-900 supported on a GC electrode in an O_2 -saturated 0.1M KOH solution at a scan rate of 10 mVs^{-1} and different rotation rates; (c) Koutecky-Levich plot of J^{-1} vs. $\omega^{-1/2}$ at -0.4 V obtained from (b); and (d) Electrochemical activity given as the kinetic-limiting current density (J_k) at -0.4 V for Pt/C, rGO, and all three NG electrodes.

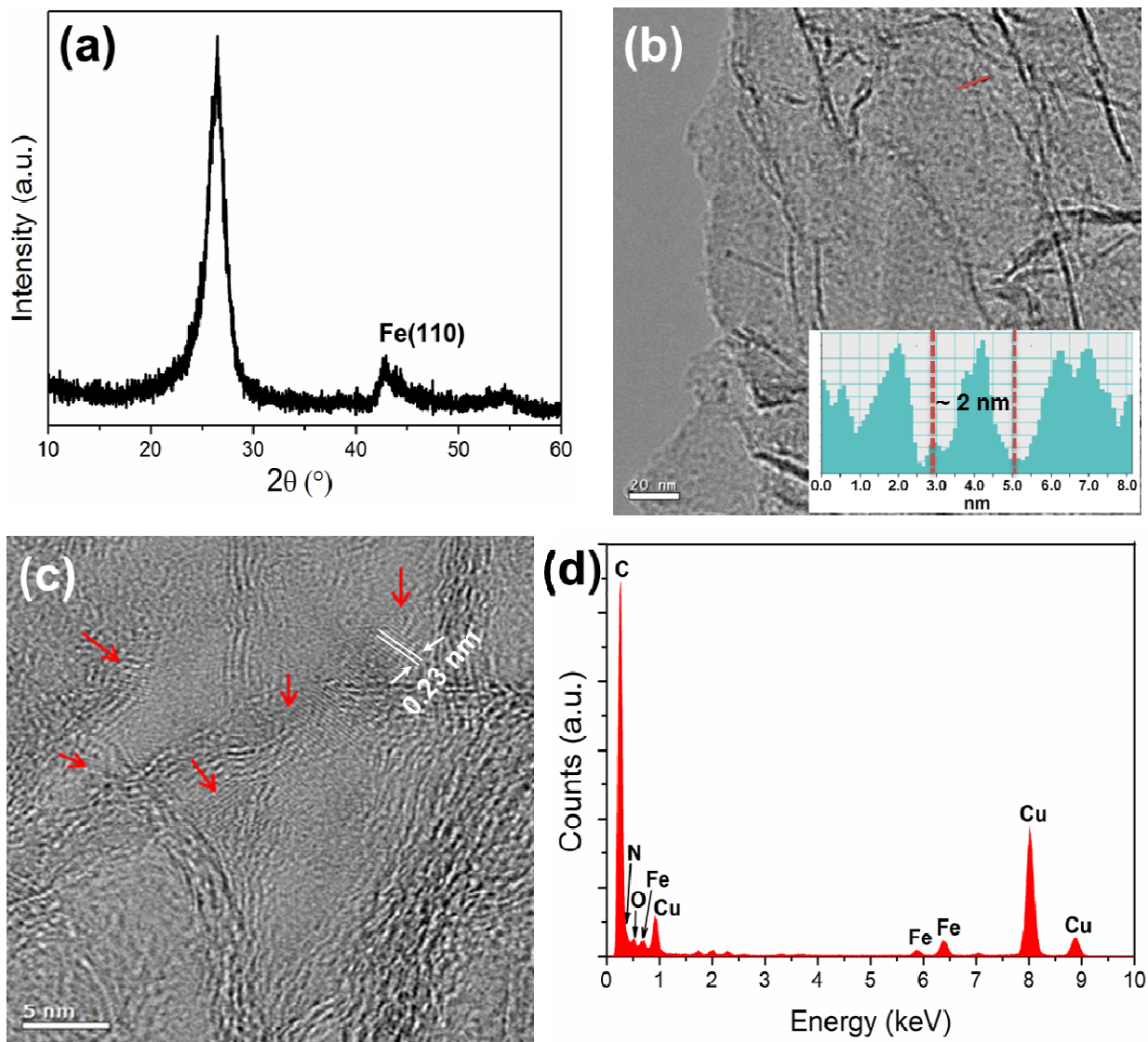


Figure 6: (a) XRD pattern of NG/Fe_{5.0} composite, (b) TEM image of NG/Fe_{5.0} with particle size distribution of the area indicated by small red line (inset), (c) HRTEM images of NG/Fe_{5.0} showing the presence of crystalline Fe nanoparticles (indicated by arrows) on NG; and (d) corresponding EDX spectra of NG/Fe_{5.0}.

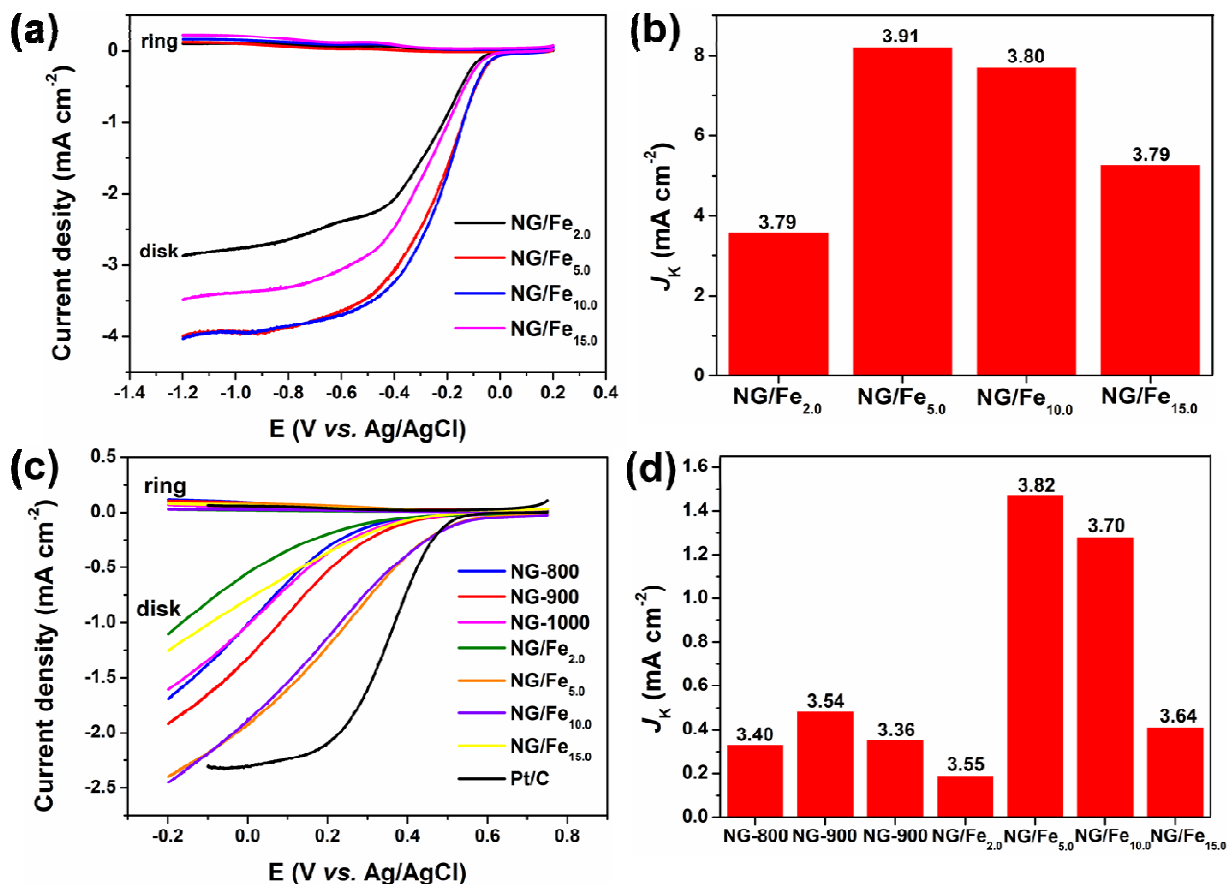


Figure 7: (a) RRDE polarization curves of NG/Fe_x samples in O₂ saturated 0.1M KOH at a scan rate of 10 mVs⁻¹ and 1600 rpm electrode rotation rate; (b) Electrochemical activity given as the kinetic-limiting current density (J_K) of the NG/Fe_x series supported on GC electrodes at -0.4 V; (c) RRDE curves of NG and NG/Fe_x series in O₂-saturated 0.5M H₂SO₄ at a scan rate of 10 mVs⁻¹ and 1600 rpm electrode rotation rate; and (d) Electrochemical activity given as the kinetic-limiting current density (J_K) of NG and NG/Fe_x series supported on GC electrodes at 0.2 V. The electron transferred number (n) in (b) and (d) was obtained from RRDE.

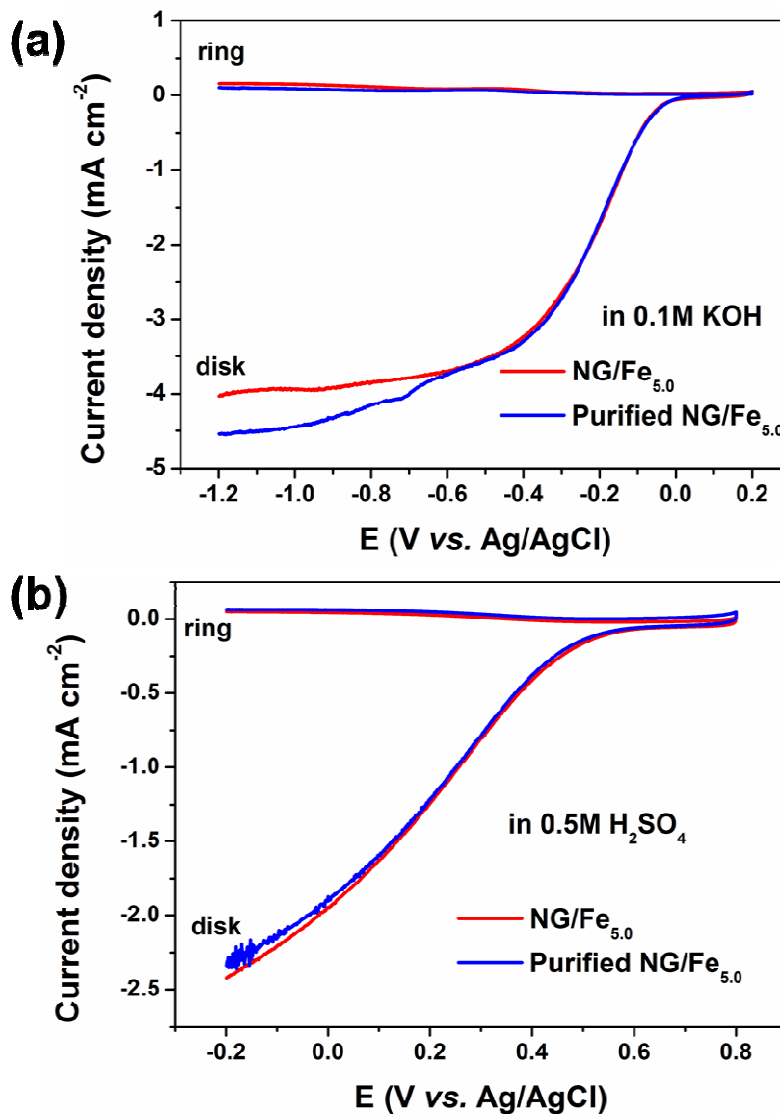


Figure 8: RRDE polarization curves of purified and unpurified NG/Fe_{5.0} in O₂-saturated (a) 0.1M KOH and (b) 0.5M H₂SO₄ solution at a rotation rate of 1600 rpm.

ToC image

